Nematic–smectic-*A* phase boundary of ideally oriented Gay-Berne system: Local density functional versus isothermal-isobaric Monte Carlo simulation

W. Józefowicz, G. Cholewiak, and L. Longa
Marian Smoluchowski Institute of Physics, Department of Statistical Physics, and Mark Kac Complex Systems Center, Jagellonian University, Reymonta 4, Kraków, Poland
(Received 14 September 2004; published 21 March 2005)

The main focus of the present paper is on studying the nematic–smectic-*A* phase boundary of an ideally oriented Gay-Berne system. The phase diagram is determined by means of an isothermal-isobaric Monte Carlo simulation. The results are compared with predictions of the local density functional expanded up to second and third order in the one-particle distribution function. It is shown that generally the second-order expansion does not give satisfactory predictions for smectics. Going beyond the leading order yields good quantitative agreement at moderate densities. With increasing density the relative error of the local density functional calculations increases, but usually does not exceed 10% in densities. We conclude that the density functional approach could be competitive to time-consuming simulations in determining phase diagrams of spatially and orientationally ordered liquid crystalline structures.

DOI: 10.1103/PhysRevE.71.032701 PACS number(s): 61.30.−v, 64.70.Md, 61.20.Ja, 61.20.−p

Monte Carlo (MC) and molecular dynamics simulations are extremely powerful techniques in gaining insight into liquid crystalline behavior. They allow one to obtain numerically exact results for problems that would otherwise require approximate methods, often of uncertain validity. Among such methods is, e.g., the widely used classical mean field theory.

A starting point of the simulations and of approximate theories is the definition of interparticle interactions. For liquid crystals, four broad classes of pair interactions have been discussed in the literature. These include (a) Lebwohl-Lasher lattice systems [1–3], (b) hard particle models [4–6], (c) single site soft potentials, where the most popular is a nonspherical version of the Lennard-Jones potential, also known as the Gay and Berne interaction [7–13], and (d) atomistic models [14].

Among the models mentioned, the Gay-Berne potential appears remarkably successful in computer modeling of liquid crystalline behavior with predictions being in line with what is observed for real mesogens. The most thoroughly documented case is the one defined by the length-to-breadth ratio of 3:1, the well depth anisotropy ratio of 5:1, and the exponents $\mu=2$ and $\nu=1$ [8]. Its potential energy contours for the long molecular axes parallel to each other are shown in Fig. 1. The complete phase diagram is found in [8], revealing isotropic liquid, nematic, and solid (also often referred to as crystalline smectic-*B*) phases. In this paper we report on combined MC isothermal-isobaric ensemble simulation and local density functional analysis of the perfectly aligned Gay-Berne system interacting through the potential shown in Fig. 1. We assume that the translational degrees of freedom of the molecules are unrestricted but their orientations are fixed parallel to the *z* axis of the laboratory frame. That is, the nematic phase is the reference state of the system with the nematic director being along *z*. Interestingly, with this restriction the smectic-$A(S_A)$ phase appears stable, Figs. 2–4, in addition to the previously mentioned nematic (N) phase and the crystalline smectic-$B(\mathrm{Cr}_B)$ phase, reported in [8] as solid. Cr_B appears stable down to $T=0$ and is composed of layers with, on the average, hexagonal distribution of the molecular centers of mass within the layer.

Our goal is to study the restricted model to test the predictive power of the local density functional theory when applied to smectics. Due to limitations imposed on molecular orientations the density functional calculations are easily carried out to orders higher than the leading one. Perhaps we should add that the simplification of the ideal nematic order certainly gives a qualitatively correct insight into liquid crystalline ordering. This has been demonstrated in the literature

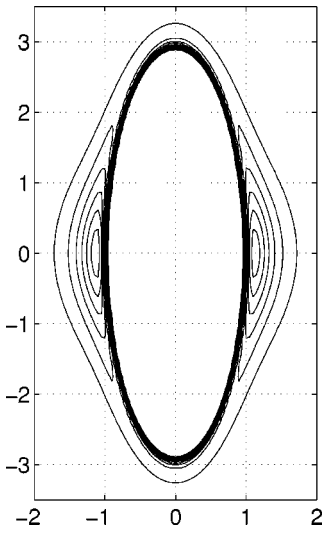

FIG. 1. The potential energy contours of the Gay-Berne interaction for a pair of ideally oriented molecules of length-to-breadth ratio 3:1. The molecules are assumed to be parallel to the *z* axis of the laboratory frame. The well depth anisotropy ratio of the potential is 5:1 and the exponents μ and ν have the values 2 and 1, respectively [8,12,13]. The contours are shown for values of the potential between 5 and 2, in steps of 0.25 [13]. Numbers are given in reduced units.

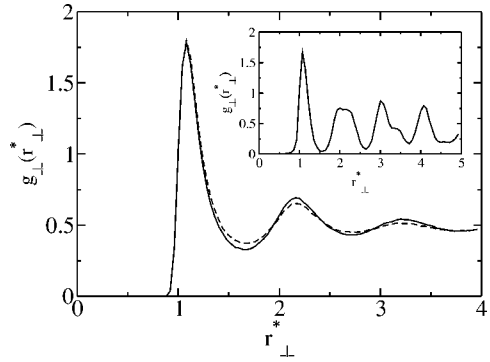

FIG. 2. Transversal positional correlation function $g_\perp(r^*_\perp)$ at $T^*=1.1$ and different pressure values. Continuous line corresponds to S_A phase ($P^*=0.5, \tau_1=0.3$), dashed line is taken in N phase ($P^*=0.4, \tau_1 \approx 0.05$), and inset shows $g_\perp(r^*_\perp)$ in Cr_B phase ($P^*=0.9, \tau_1=0.8$).

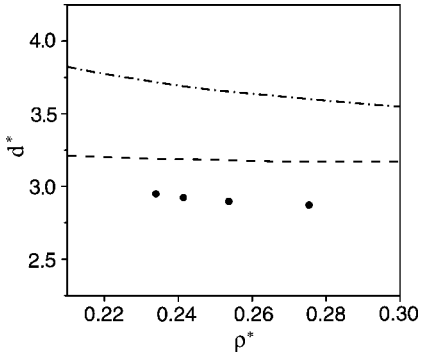

FIG. 4. Layer thickness versus ρ^* of S_A phase obtained from simulations (solid circles) and by means of local density functional theory. d^* is shown at N-S_A transition for points represented by solid circles in Fig. 3. Lines depict results for second- (-·-·-·-) and third- (-----) order local density functional calculations.

for the nematic phase [15,16] and for polar ordering in smectic phases [12,13] of perfectly oriented Gay-Berne systems. Also more general models of smectic ordering [17] and studies of anchoring [18] have proved usefulness of such modeling.

We performed isothermal-isobaric Monte Carlo simulations in a standard way [19,20] for a system consisting of 600 ideally oriented Gay-Berne molecules, Fig. 1. A reduced system of units has been used as defined in [8,11–13] and given in the Appendix. Although a standard cutoff at the reduced distance of 4 was applied, the effect of the potential tail has been taken into account by evaluating long-range

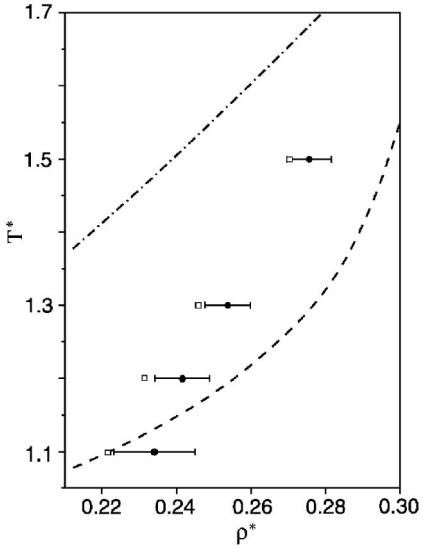

FIG. 3. Phase diagram obtained from simulations and by means of local density functional theory in plane of reduced density (ρ^*) and temperature (T^*). Lines depict boundary between nematic and smectic-A phases obtained up to second (-·-·-·-) and third (-----) order of local density functional expansion. Points refer to the same phase boundary from *NPT* Monte Carlo simulation: open squares correspond to the phase diagram without long-range corrections and solid circles represent diagram after taking into account long-range corrections. Solid circles are shown together with the corresponding error bars. Stable smectic-A phase appears at higher densities.

corrections [19,20]. Starting from the nematic phase at $T^*=1.1$ and reduced pressure of $P^*=0.2$ the system was next compressed with the pressure step of 0.1 until a stable smectic-A phase was obtained. The reverse process showed no hysteresis indicating that the phase transition to the smectic-A phase was second order. The maximal trial particle move did not exceed 0.2 (in reduced units) and was adjusted during simulation to guarantee the acceptance ratio of 0.5. Each cycle was followed by trial changes of the system box sides. The number of cycles needed to equilibrate the system was approximately 100 000. The production run took another 100 000–200 000 cycles with particle configurations being saved every 100 cycles.

The smectic-A structure has been identified by calculating the translational order parameter along the z axis [13,21]

$$\tau_1 = |\langle \exp(2\pi i z^*/d^*) \rangle|, \tag{1}$$

where z^* is the reduced coordinate along the director and d^* is the smectic layer spacing. The *NPT* ensemble thermodynamic average is denoted by $\langle \cdots \rangle$. The initially unknown layer spacing is adjusted by maximizing the translational order parameter with respect to d^*. Clearly, for the ideal nematic liquid $\tau_1=0$ while for the ideal smectic-A phase $\tau_1=1$. Owing to the finite size of the system τ_1 is nonzero in the nematic phase as well, but the fluctuations of τ_1 in the nematic phase were found to be relatively small and oscillate between 0.04 and 0.09.

The other useful quantity monitored was the pair distribution function [13,22]

$$g(\mathbf{r}^*) = \frac{V^*}{N^2} \left\langle \sum_i \sum_{j \neq i} \delta(\mathbf{r}^* - \mathbf{r}_i^* + \mathbf{r}_j^*) \right\rangle. \tag{2}$$

For the smectic-A ordering it is sufficient to consider only longitudinal and transversal components of g with respect to the director [13]. They are denoted $g_\parallel(r^*_\parallel)$ and $g_\perp(r^*_\perp)$, respectively. Note that $g_\parallel(r^*_\parallel)$ provides an alternative way of determining d^* while $g_\perp(r^*_\perp)$ allows one to distinguish between the S_A and Cr_B phases. The typical behavior of $g_\perp(r^*_\perp)$ in N, S_A, and Cr_B phases is shown in Fig. 2. The phase diagram obtained from simulations (Fig. 3) is compared with predic-

tions of the density functional theory (DFT). According to that theory [23–26] the grand potential $\Omega[\rho]$ of liquid crystals is a functional of the one-particle distribution function $\rho(i)$. In the absence of an external field the expression for $\Omega[\rho]$ reads

$$\Omega[\rho] = \mathcal{F}[\rho] - \mu \int d(i)\rho(i), \tag{3}$$

where i denotes all single particle coordinates and where the free energy $\mathcal{F}[\rho]$ is given by

$$\beta\mathcal{F}[\rho] = \int d(i)\rho(i)\{\ln \Lambda^3\rho(i) - 1\} - \Phi[\rho]. \tag{4}$$

Here Λ comes from the integration over momenta.

The first part of Eq. (4) represents the free energy of the noninteracting gas of particles. The most important is the excess part denoted by $\Phi[\rho]$. Here we approximate $\Phi[\rho]$ by means of the Mayer expansion [27]

$$\Phi[\rho] = \frac{1}{2!}\int\int d(1)d(2)f(1,2)\rho(1)\rho(2) + \frac{1}{3!}\int\int\int d(1)d(2)d(3)f(1,2)f(2,3)f(1,3) \times \rho(1)\rho(2)\rho(3) + \cdots, \tag{5}$$

where f is the Mayer function, $f(i,j) = e^{-\beta V(i,j)} - 1$, and $V(i,j)$ is the pair potential. The equilibrium distribution function $\rho(i)$ is found from the functional minimization of Ω with respect to ρ subject to the normalization condition [27]. The necessary condition for a minimum is given in the form of the nonlinear integral equation

$$\rho(i) = \mathcal{N}\exp\left[\frac{\delta\Phi[\rho]}{\delta\rho(i)}\right], \tag{6}$$

where $\mathcal{N}$ is the normalization constant.

The continuous nematic–smectic-A phase transition can be found from Eq. (6) by performing a bifurcation analysis of Eq. (6) about the reference nematic state. Choosing $\rho(i) \equiv \rho(z^*) = \rho_0^*(1 + 2\tau_1\cos(2\pi z^*/d^*) + \cdots)$, we find that the nematic–smectic-A phase boundary must satisfy the equation

$$1 = \rho_0^* \int d\mathbf{r}^{*\prime} f(\mathbf{r}^{*\prime})\cos\left(\frac{2\pi}{d^*}z^{*\prime}\right) + (\rho_0^*)^2 \int d\mathbf{r}^{*\prime} d\mathbf{r}^{*\prime\prime} \times f(\mathbf{r}^{*\prime})f(\mathbf{r}^{*\prime\prime} - \mathbf{r}^{*\prime})f(\mathbf{r}^{*\prime\prime})\cos\left(\frac{2\pi}{d^*}z^{*\prime\prime}\right) + \cdots, \tag{7}$$

where $f(i,j) \equiv f(\mathbf{r}^*, \mathbf{r}^{*\prime}) = \exp[-U_{GB}^*(\mathbf{r}^{*\prime} - \mathbf{r}^*)/T^*] - 1$ and where U_{GB}^* represents the Gay-Berne potential (expressed in reduced units). Equation (7) links T^*, d^*, and ρ_0^*. For fixed ρ_0^* the maximal T^* as a function of d^* determines the transition temperature and the equilibrium layer spacing. The corresponding equilibrium pressure is found from ordinary thermodynamic relations [27]. The phase diagram evaluated with the help of Eq. (7) is shown in Fig. 3, where the full third-order density functional analysis (dashed line) is compared with the calculations that go only to leading order in density [i.e., with the $(\rho_0^*)^2$ term in Eq. (7) being disregarded], and with a computer simulation. The layer thickness resulting from DFT and simulations is shown in Fig. 4. Please note that at low temperatures the agreement between the third-order calculations and simulations is within experimental error (except for d^*) while generally the discrepancy does not exceed 10%. We should mention that the ordinary mean field analysis yields the relative error of 30%–50% for nematics and is not fully conclusive for smectics as it usually does not provide the equilibrium value for d^*.

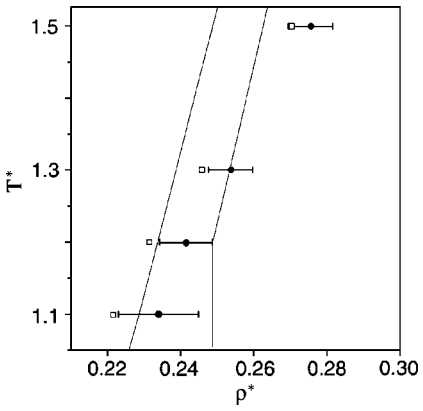

FIG. 5. Comparison between phase diagram of ideally aligned Gay-Berne system with $\kappa = 3.0$ (points) and the unrestricted Gay-Berne system of molecules with length-to-breadth ratio 3.8:1 (taken from Ref. [10]). Only a part of the diagram with the stable smectic-A island is shown.

Interestingly, in simulations of de Miguel and Vega [8] no stable S_A phase has been detected. Freezing the orientational degrees of freedom enhances the stability of S_A with respect to N and Cr_B and, eventually, makes S_A stable in a limited range of temperature and density. We would like to add that a quite similar phase boundary between nematic and smectic-A phases was found for an orientationally unrestricted model, but with a slightly larger shape anisotropy [10] (see Fig. 5). Thus, we could speculate that the effect of restricting orientations is partly compensated by going to more anisotropic molecules. Also it shows that release of geometrical restriction and switching on an external electric (magnetic) field instead would stabilize the field-induced nematic–smectic-A phase transition in the model studied.

Finally, we should mention that the qualitatively correct results obtained with the density functional expansion indicate the possibility of constructing a hybrid method that would combine computer simulation with density functional theory to study phase diagrams of complex fluids. For instance, computer simulation data (singlet and pair distribution functions) in the isotropic or nematic phase could be used as input to construct a density functional expansion. Subsequent application of the bifurcation theory would then allow for predictions about more ordered phases, like smectics. Atomistic simulations, which are still at the preliminary stage, seem natural candidates for practical use of the hybrid method. Its construction is currently under way and the results will be presented in our forthcoming publication.

This work was supported by the Polish (KBN) Project No. 5 P03B 052 20. We also gratefully acknowledge the KBN

computing grant (No. KBN/SGI2800/UJ/025/2003) toward the use of the ACK Cyfronet (Kraków) computers.

APPENDIX: REDUCED UNITS

It is convenient to define the dimensionless (reduced) units of distance and energy in terms of the Gay-Berne potential parameters σ_0 and ε_0 [13], which correspond to the contact separation and the well depth for a pair of molecules in the cross arrangement (i.e., when all scalar products between the vectors describing molecular orientations and the separation vector vanish). The dimensionless reduced units (denoted by an asterisk) of other quantities can be derived yielding distance $r^*=r/\sigma_0$, energy $U^*=U/\varepsilon_0$, temperature $T^*=k_BT/\varepsilon_0$, density $\rho^*=\rho\sigma_0^3$, and pressure $P^*=P\sigma_0^3/\varepsilon_0$.

[1] P. A. Lebwohl and G. Lasher, Phys. Rev. A **6**, 426 (1972).
[2] U. Fabbri and C. Zannoni, Mol. Phys. **58**, 763 (1986).
[3] F. Biscarini, C. Chiccoli, P. Pasini, F. Semeria, and C. Zannoni, Phys. Rev. Lett. **75**, 1803 (1995).
[4] D. Frenkel, Mol. Phys. **60**, 1, (1987).
[5] D. Frenkel, H. N. W. Lekkerkerker, and A. Stroobants, Nature (London) **332**, 822 (1988).
[6] J. A. C. Veerman and D. Frenkel, Phys. Rev. A **41**, 3237 (1990).
[7] J. G. Gay and B. J. Berne, J. Chem. Phys. **74**, 3316 (1981).
[8] E. de Miguel, C. Vega, J. Chem. Phys. **117**, 6313 (2002).
[9] J. Stelzer, L. Longa, and H.-R. Trebin, Phys. Rev. E **55**, 7085 (1997).
[10] J. T. Brown, M. P. Allen, E. M. del Río, and E. de Miguel, Phys. Rev. E **57**, 6685 (1998).
[11] M. A. Bates and G. R. Luckhurst, J. Chem. Phys. **110**, 7087 (1999).
[12] L. Longa, G. Cholewiak, and J. Stelzer, Acta Phys. Pol. B **31**, 801, (2000).
[13] L. Longa, H.-R. Trebin, and G. Cholewiak, in *Relaxation Phenomena: Liquid Crystals, Magnetic Systems, Polymers, High-T_c Superconductors, Metallic Glasses*, edited by W. Haase and S. Wróbel (Springer-Verlag, Heidelberg, 2003), pp. 204–233.
[14] M. J. Cook and M. R. Wilson, Liq. Cryst. **27**, 1573 (2000).
[15] W. L. Wagner, Mol. Cryst. Liq. Cryst. **299**, 33 (1997).
[16] W. L. Wagner and L. Bennett Mol. Phys. **94**, 571 (1998).
[17] P. I. C. Teixeira, M. A. Osipov, and M. M. Telo da Gama, Phys. Rev. E **57**, 1752 (1998).
[18] M. A. Osipov, T. J. Sluckin, and S. J. Cox, Phys. Rev. E **55**, 464 (1997).
[19] M. P. Allen and D. J. Tildesly, *Computer Simulation of Liquids* (Clarendon, Oxford, 1987).
[20] D. Frenkel and B. Smit, *Understanding Molecular Simulation: From Algorithms to Applications*, 2nd ed. (Academic Press, San Diego, 2001).
[21] P. J. Wojtowicz, in *Introduction to Liquid Crystals*, edited by E. B. Priestley, P. J. Wojtowicz, and P. Sheng (Plenum, New York, 1974), Chap. 7.
[22] C. Gray and K. E. Gubbins, *Theory of Molecular Fluids* (Clarendon, Oxford, 1984).
[23] J. P. Hansen, *Observation, Prediction and Simulations of Phase Transitions in Complex Fluids* (Kluwer, Dordrecht, 1995).
[24] A. D. J. Haymet and D. W. Oxtoby, J. Chem. Phys. **84**, 1769, (1986).
[25] J. L. Barrat, J. P. Hansen, and G. Pastore, Phys. Rev. Lett. **58**, 2075 (1987).
[26] R. Evans, Adv. Phys. **28**, 143 (1979).
[27] J. P. Hansen and I. R. McDonald, *Theory of Simple Liquids* (Academic Press, London, 1981).